J Oceanogr (2013) 69:527–544
DOI 10.1007/s10872-013-0190-8

ORIGINAL ARTICLE

Modeling the long-term variability of phytoplankton functional groups and primary productivity in the South China Sea

Wentao Ma · Fei Chai · Peng Xiu · Huijie Xue · Jun Tian

Received: 3 December 2012 / Revised: 18 June 2013 / Accepted: 21 June 2013 / Published online: 11 July 2013

Abstract Primary productivity (PP) and phytoplankton structure play an important role in regulating oceanic carbon cycle. The unique seasonal circulation and upwelling pattern of the South China Sea (SCS) provide an ideal natural laboratory to study the response of nutrients and phytoplankton dynamics to climate variation. In this study, we used a three-dimensional (3D) physical–biogeochemical coupled model to simulate nutrients, phytoplankton biomass, PP, and functional groups in the SCS from 1958 to 2009. The modeled results showed that the annual mean carbon composition of small phytoplankton, diatoms, and coccolithophores was 33.7, 52.7, and 13.6 %, respectively. Diatoms showed a higher seasonal variability than small phytoplankton and coccolithophores. Diatoms were abundant during winter in most areas of the SCS except for the offshore of southeastern Vietnam, where diatom blooms occurred in both summer and winter. Higher values of small phytoplankton and coccolithophores occurred mostly in summer. Our modeled results indicated that the seasonal variability of PP was driven by the East Asian Monsoon. The northeast winter monsoon results in more nutrients in the offshore area of the northwestern Luzon Island and the Sunda Shelf, while the southwest summer monsoon drives coastal upwelling to bring sufficient nutrients to the offshore area of southeastern Vietnam. The modeled PP was correlated with El Niño/Southern Oscillation (ENSO) at the interannual scale. The positive phase of ENSO (El Niño conditions) corresponded to lower PP and the negative phase of ENSO (La Niña conditions) corresponded to higher PP.

Keywords Phytoplankton functional groups · Primary productivity · Nutrient dynamics · East Asian Monsoon · ENSO · South China Sea · ROMS–CoSiNE model

1 Introduction

The South China Sea (SCS, 0°–25°N, 100°–125°E) is the largest marginal sea in the northwestern Pacific. The atmospheric circulation of the SCS is strongly controlled by the East Asian Monsoon (EAM). Seasonal wind prevails with northeasterlies in winter and southwesterlies in summer. April to May and September are two transition periods that punctuate the alternation of winter and summer monsoon (Liu et al. 2004; Xie et al. 2003). The geometry of the SCS leads to widespread upwelling and seasonal variation of surface circulation under the influence of the EAM. The prevailing northeast monsoon results in a basin-wide cyclonic surface circulation, and the southwest monsoon causes a surface circulation dipole: a cyclonic gyre in the north and an anticyclonic gyre in the south (Su 2004). Meanwhile, the Ekman transport drives the upwelling off southeastern Vietnam in summer (Kuo et al. 2000; Xie et al. 2003), and off northwestern Luzon Island, as well as the northern Sunda Shelf, in winter (Liu et al. 2002; Shaw et al. 1996). Cold deep waters that enter the SCS through Luzon Strait (LS) need to upwell and flow laterally

W. Ma (✉) · J. Tian
State Key Laboratory of Marine Geology, Tongji University, 1239 Siping Road, Shanghai 200092, China
e-mail: wtma@tongji.edu.cn

W. Ma
College of Environmental Science and Engineering, Tongji University, Shanghai 200092, China

F. Chai · P. Xiu · H. Xue
School of Marine Sciences, The University of Maine, Orono, ME 04469, USA

somewhere to compensate for the descending movement (Qu et al. 2009). Therefore, the SCS is a basin-wide upwelling system. The residence time of deep water is only 30–150 years, which results in a high upwelling rate and a shallow nutricline (Wong et al. 2007a). This featured upwelling and seasonal circulation pattern is crucial to the nutrient dynamics and biogeochemistry in the SCS.

Phytoplankton, the primary producer of organic matter, plays an important role in regulating oceanic carbon cycles. In the SCS, many observations have indicated that the growth of phytoplankton responds sensitively to the monsoon-related physical-biogeochemical processes. The northeast winter monsoon results in an enhanced mixing of the entire basin, which increases the overall nutrient supply and primary productivity (PP) in the euphotic zone (Liu et al. 2002; Palacz et al. 2011; Tseng et al. 2005; Wang et al. 2010; Wong et al. 2007b). The southwest summer monsoon, however, only results in an enhanced PP in the offshore area of southeastern Vietnam (Kuo et al. 2000) and the southern SCS (Ning et al. 2004). This unique seasonality of PP also affects the efficiency of POC export. Particle flux from sediment traps showed annual or semi-annual cycles that responded to the EAM change (Chen et al. 2007a; Lahajnar et al. 2007; Wan et al. 2010; Wei et al. 2011).

It has also been found that the nutrient supply is important to the variability of the phytoplankton community structure. Diatoms grow better in less stratified and nutrient-rich conditions, while picoplankton are dominant when the surface water is stratified and under oligotrophic conditions (Iglesias-Rodríguez et al. 2002; Litchman et al. 2007; Margalef 1978). Chen et al. (2007b) indicated that the alternating dominancy between coccolithophores and diatoms in the northern SCS revealed the EAM-driven nutrient dynamics. A rare basin-scale survey conducted by Ning et al. (2004) in 1998 also showed a significant variation of the phytoplankton community. However, a very strong El Niño event occurred in 1998, during which both the winter and summer monsoons weakened significantly (Lan et al. 2012; Xie et al. 2003, 2009). Chlorophyll-*a* (Chl-*a*) concentration in the summer of 1998 was the lowest in the western SCS from 1997 to 2004 (Zhao and Tang 2007). Limited observations may be biased because of under sampling in space and time, adding uncertainties to the biomass and PP estimations. Physical-biogeochemical modeling thus becomes a versatile tool to bridge the gap and to investigate nutrient and phytoplankton dynamics in responding to the EAM change on the basin scale.

In the SCS, numerical modeling that focuses on biogeochemical processes is still limited compared to physical oceanographic modeling. Examples of the latter include Chao et al. (1996), Metzger and Hurlburt (1996), Xue et al. (2004), and Wang et al. (2011). Liu et al. (2002) was the first to model chlorophyll and PP responses to the EAM using a simple "nutrient/phytoplankton/zooplankton/detritus" (NPZD) model. Recently, more sophisticated three-dimensional (3D) physical-biogeochemical models have been developed to study the spatial and long-term variation of PP, export production, and air–sea CO_2 exchange (Chai et al. 2009; Liu and Chai 2009). The previous studies, however, did not discuss the variability of the phytoplankton community in the SCS. The current knowledge on the phytoplankton community suggests that small and large phytoplankton differ in sinking, remineralization, and growth rates. Calciferous phytoplankton and non-calciferous phytoplankton also differ in the functioning of the biological carbon pump. One numerical modeling example in the Atlantic Ocean argued that the coccolithophores to diatoms ratio increased by 80 % under a global warming scenario, which is a positive feedback (outgassing of CO_2 during calcification) to the increasing atmospheric pCO_2 (Cermeño et al. 2008). In this paper, we updated the carbon $Si(OH)_4$ nitrogen ecosystem (CoSiNE) model (Chai et al. 2002) by adding a calciferous functional group (coccolithophores) to the model (Fujii and Chai 2007), which allowed us to simulate a long-term variability of phytoplankton biomass and PP as well as dynamic changes of functional groups in the SCS.

The rest of this paper is organized as follows. In Sect. 2, the regional ocean model system (ROMS)-CoSiNE model is briefly introduced. Section 3.1 compares the model results with observations. In Sects. 3.2–3.4, the spatial distribution of modeled phytoplankton, seasonal variation, and interannual variations are discussed.

2 Model and data

2.1 Model description

We used a 3D coupled physical-biogeochemical model in this study. The physical model was based on the ROMS which was a free-surface, terrain-following, primitive equation ocean model. The Pacific Ocean (45°S–65°N, 99°E–70°W) configuration by Wang and Chao (2004) was adopted in this study. The model has a horizontal resolution of 50 km in both zonal and meridional direction and 20 levels in the vertical. The northern and southern boundaries of the model are closed walls. A sponge layer was applied to temperature, salinity, and nutrients. The treatment of the sponge layer consisted of a decay term $\kappa(T^* - T)$, $\kappa(S^* - S)$, and $\kappa(N^* - N)$ in the temperature, salinity, and nutrient/carbon equations, respectively, which restored the modeled variables to the observed temperature T^*, salinity S^*, and nutrients N^* fields at the two closed walls. The value of κ varied smoothly from 1/30 day^{-1} at the walls to zero at 5° from the walls.

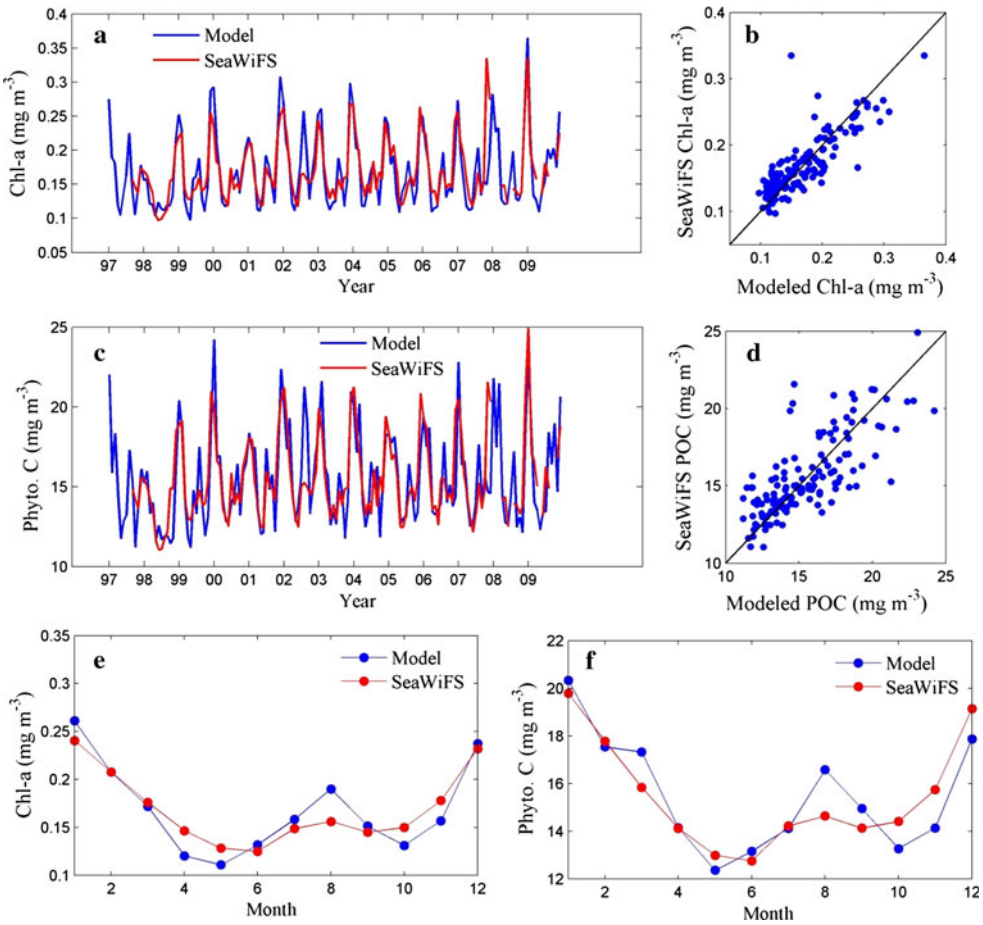

Fig. 1 Modeled Chl-a and POC in comparison with the corresponding SeaWiFS satellite data. **a** Time series of modeled and SeaWiFs Chl-a from 1997 to 2009. **b** Scatter plot of the modeled versus SeaWiFs Chl-a. **c** Time series of modeled and SeaWiFs POC from 1997 to 2009. **d** Scatter plot of the modeled versus SeaWiFs POC. **e–f** Comparison of climatological Chl-a and POC with the corresponding SeaWiFS data. *Diagonals* in (**b**) and (**d**) are 1:1 lines. SeaWiFS POC is divided by 3.2

The biogeochemical scheme is based on the CoSiNE model developed by Chai et al. (2002) and Dugdale et al. (2002), in which the phytoplankton community was represented by a small number of functional groups rather than individual taxonomies for the sake of applicability and computation efficiency. After introducing a calciferous functional group into the CoSiNE model, the updated model includes four nutrients [silicate (SiO_4), nitrate (NO_3), ammonium (NH_4) and dissolved inorganic carbon, (DIC)], three phytoplankton groups [small phytoplankton (P1), diatoms (P2), and coccolithophores (P3)], two grazers [microzooplankton (Z1) and mesozooplankton (Z2)], and four detrital pools [detritus nitrogen (DN), detritus silicate (DSi), detritus carbon (DC), and detritus calcium carbonate (DCa)].

In the euphotic zone, the growth rate of the phytoplankton is determined by the Michaelis–Menten type feedback in order to take nutrient limitation into account (Dugdale 1967). P1, P2, and P3 assimilate DIC and dissolved inorganic nitrogen (DIN) to form organic matters. Silicate and DIC are absorbed by P2 and P3, respectively, to form silica and calcium carbonate shells. The ratio of calcium carbonate to organic carbon is set to unity during P3 calcification. Z1 only graze on P1 that is a non-sinking group, while Z2 graze on P2 and P3 and prey on Z1 and DC. Below the euphotic zone, sinking particulate organic matters are converted to inorganic nutrients by a regeneration process, in which organic nitrogen decays to ammonium and then is nitrified to nitrate. The degradation rates for particulates are functions of temperature. A brief introduction of equations and parameters are given in the "Appendix". Readers are also referred to Xiu and Chai (2012) for detailed implementations of the model.

It is worth noting that the treatment of three major functional groups is a model simplification rather than the realistic phytoplankton community structure. Nevertheless, this coccolithophores-included model is more comprehensive for the SCS which is a calcium carbonate well-preserved basin (Wang and Li 2009). Fujii et al. (2007) also indicated that the introduction of coccolithophores into the model relaxed the grazing pressure on the diatoms and increased diatom biomass. Liu et al. (2002) incorporated the photo-adaptation into the NPZD model with one phytoplankton functional group, and argued that it is necessary to use a variable Chl-a to nitrogen (Chl-a/N) ratio in order to reproduce the subsurface chlorophyll maximum (SCM)

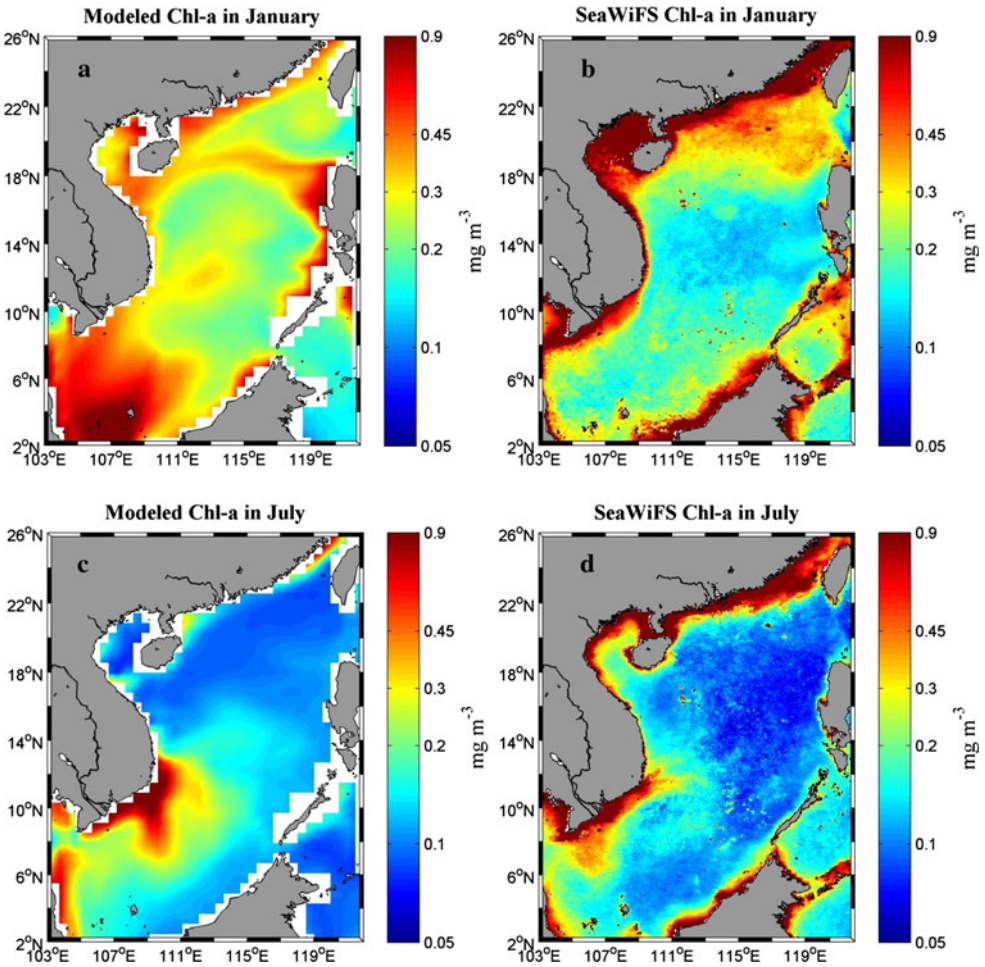

Fig. 2 Comparison between the modeled and SeaWiFS Chl-a: **a**, **b** in January, **c**, **d** in July

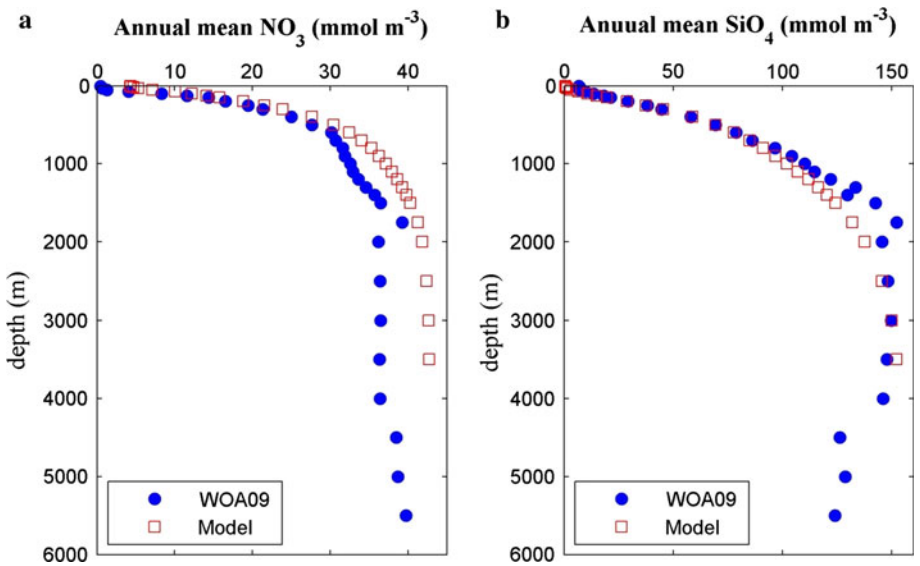

Fig. 3 Depth profile of the modeled annual mean **a** NO_3 and **b** SiO_4, compared with the WOA 2009 data (Garcia et al. 2010)

(Liu et al. 2007b). In the current ROMS–CoSiNE model, the Chl-a, nitrogen, and carbon of the phytoplankton were incorporated as independent variables. Thus, we were able to take a variable C/N and C/Chl-a molar ratio in the production of organic matter rather than a fixed Redfield ratio (Fujii and Chai 2007).

In this study, the model was initialized with climatological temperature, salinity, and nutrients from the World Ocean Atlas

Table 1 Annual mean and range (in parentheses) of the biomass of three groups of phytoplankton[a] and the sum of the three

Subdomain[b]	P1 (mmol C m^{-2})	P2 (mmol C m^{-2})	P3 (mmol C m^{-2})	P1 + P2 + P3 (mmol C m^{-2})
N	33.3 (32.6–35.0)	47.5 (32.4–71.1)	22.1 (15.9–34.95)	103.0 (83.2–122.1)
NE1	40.4 (35.7–50.9)	8.5 (2.4–20.6)	41.7 (19.6–77.4)	90.6 (66.0–128.2)
NE2	36.8 (34.2–39.2)	49.3 (24.5–104.7)	21.7 (12.1–35.2)	107.8 (83.1–152.3)
C	36.7 (34.3–39.2)	68.9 (52.4–96.4)	4.8 (3.2–6.5)	110.4 (97.3–134.7)
SW	33.5 (30.9–36.1)	77.3 (56.1–100.0)	4.7 (3.7–6.5)	115.5 (98.1–138.5)
S	32.5 (29.4–35.8)	55.4 (33.9–93.8)	2.5 (0.7–4.8)	90.3 (71.2–124.0)
SCS	34.7 (33.1–35.7)	54.3 (43.7–76.5)	14.0 (8.2–22.5)	103.0 (90.0–119.1)

N Northern box, *NE1* northeastern box 1, *NE2* northeastern box 2, *C* central box, *SW* southwestern box, *S* southern box, *SCS* the entire SCS

[a] All values are the integrations from 0 to 125 m in areas with the water depth >500 m

[b] Symbols represent subdomains as in Fig. 4a

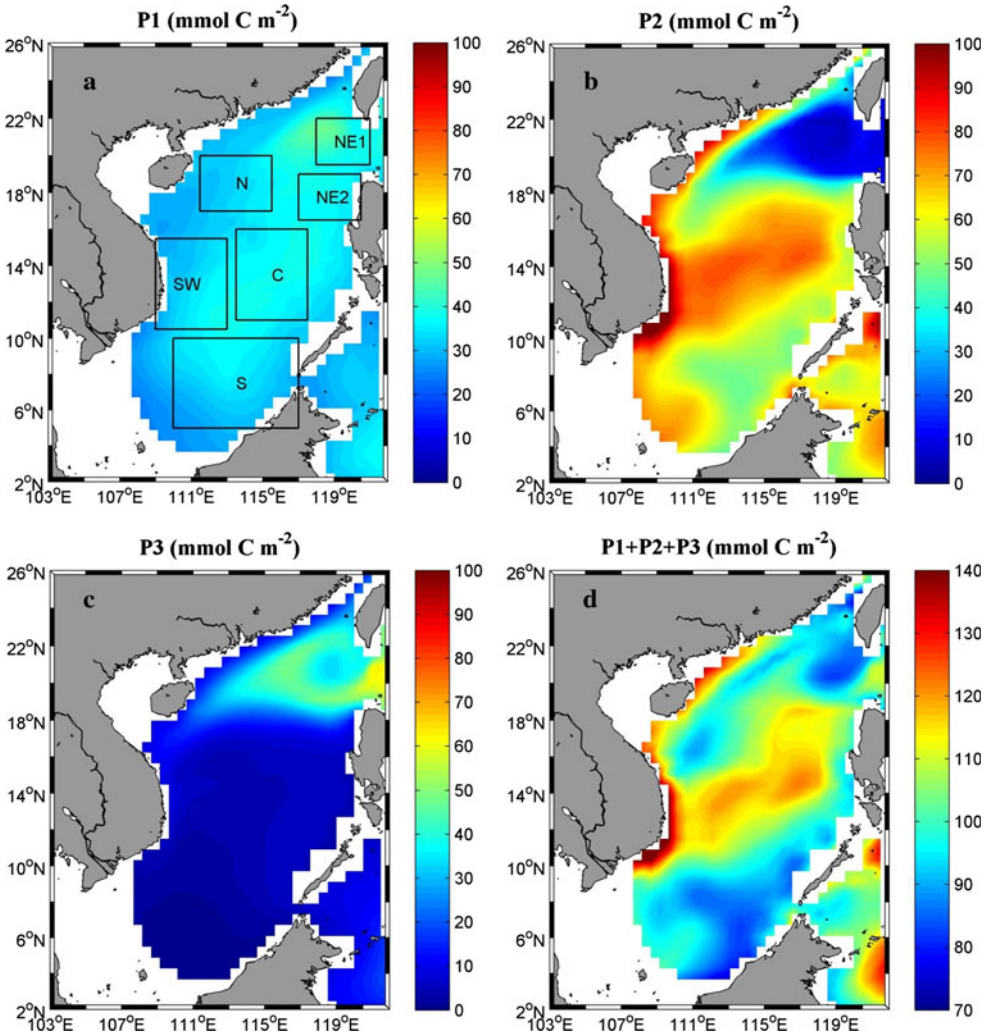

Fig. 4 Annual mean **a** small phytoplankton (P1), **b** diatom (P2), **c** coccolithophores (P3), and **d** total phytoplankton carbon (P1 + P2 + P3) integrated from 0 to 125 m. *Boxes* in (**a**) are 6 subdomains described in Table 1

(WOA) 2005 (Locarnini et al. 2006) and spun up for years to reach a quasi-equilibrium state. From this equilibrium, the ROMS–CoSiNE model was integrated for the period from 1958 to 2009 forced with daily air–sea fluxes of momentum, heat, and freshwater from the NCEP/NCAR reanalysis (Kalnay et al. 1996). River discharges were not considered in the model.

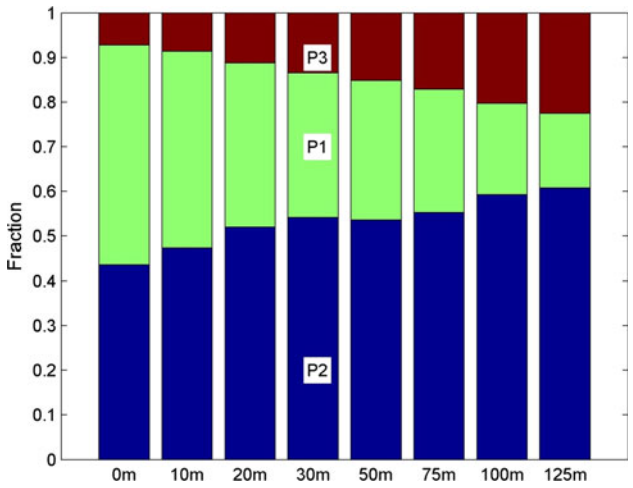

Fig. 5 Annual mean fraction of three types of phytoplankton with depth. *Red*, *green*, and *blue* represent P3, P1, and P2, respectively (color figure online)

2.2 Satellite and in situ data

Surface Chl-a and carbon data from the sea-viewing wide field-of-view sensor (SeaWiFS) project from September 1997 to December 2009 were used to evaluate the model performance. The particulate organic carbon (POC) was calculated from satellite-sensed particulate backscattering coefficient through empirical and regionally observed relationships (Behrenfeld et al. 2005). Measured annual mean climatology of nitrate (NO_3) and silicate (SiO_4) were obtained from the WOA 2009 (Garcia et al. 2010).

3 Results and discussion

3.1 Comparing modeled Chl-a, POC, and nutrients with observations

The monthly mean time series and climatological annual cycle of the modeled Chl-a and POC were calculated and compared with the SeaWiFS data for the period from 1997 to 2009. In Fig. 1, the modeled Chl-a and POC showed a high correlation with satellite derivations ($R = 0.8$, $p < 0.01$). The climatological annual cycle also indicated the consistency in both amplitude and phase (Fig. 1e, f). Chl-a and POC concentrations had two peaks in winter and summer but the former one was higher. Spring and autumn were low Chl-a and POC concentration seasons. The summer peak disappeared in 1998 due to the El Niño. All these features were reproduced well in the model. The SeaWiFS POC shown in Fig. 1c has been divided by 3.2 because phytoplankton carbon only accounted for a small fraction of the total POC. Eppley et al. (1992) reported that the phytoplankton carbon to POC (Phyto. C/POC) ratio ranged from 29 to 49 % in the equatorial Pacific. DuRand et al. (2001) found a relatively constant value of 33 % throughout the year near Bermuda. The good comparison between our modeled phytoplankton carbon and the SeaWiFS POC after division indicated a Phyto. C/POC ratio of 1:3.2 in the SCS (Fig. 1d). This validation also determined a Chl-a/C ratio of 0.008–0.014.

The modeled seasonal variation of Chl-a also shared similarity with the satellite data. Surface plots showed that the high Chl-a concentration occurred off the west coast of Luzon Island and on the Sunda Shelf in January (Fig. 2a). The central basin, however, was low in concentration. In July, high chlorophyll values were located offshore of southeastern Vietnam. The modeled result is also similar to the basin-scale survey conducted by Ning et al. (2004) in 1998 (see their fig. 5). Moreover, our model results depicted a clear phytoplankton variation which responded to the EAM. The northeast winter monsoon induces positive wind stress curls on the offshore area of the west of Luzon Island and the Sunda Shelf where upwelling brings more nutrients to support the growth of the phytoplankton. The southwest summer monsoon breeze along the coast of southeastern Vietnam causes strong Ekman transport. This prominent monsoon-driven variability of phytoplankton is consistent with previous simulations by Liu et al. (2007b, 2002).

However, a large discrepancy between the model and satellite data stand out in the northern SCS. The SeaWiFS data showed high chlorophyll concentrations off the west of LS, but the modeled chlorophyll was very low in the corresponding area (Fig. 2). Our modeled high Chl-a values only occurred off the western Luzon Island and did not extend to the north in winter. There are three potential reasons that may account for this discrepancy.

The first is the overestimated Kuroshio intrusion in the ROMS model. The cross-section at the LS showed that the surface concentration of nitrate (NO_3) and silicate (SiO_4) was lower in the western Pacific than the SCS (Chen et al. 2001). The annual mean surface SiO_4 from WOA 2009 also showed a low concentration area in the northeastern SCS, but our modeled low SiO_4 area extended more westward. The Kuroshio water has high temperature and salinity. The modeled salinity (not shown) indicated that this low SiO_4 area collocated with high salinity waters. In other words, there were surplus Kuroshio waters that intruded into the northern SCS in the model. The intruded waters with low concentration of nutrients would limit the growth of phytoplankton in the current model configuration. Except for the northern part, modeled higher SiO_4 values are consistent with WOA 2009 in the central basin. The basin-averaged depth profiles of the modeled nutrients are also consistent with observations (Fig. 3).

The second reason for the discrepancy is the lack of river sources. Pearl River, the largest river in the northern

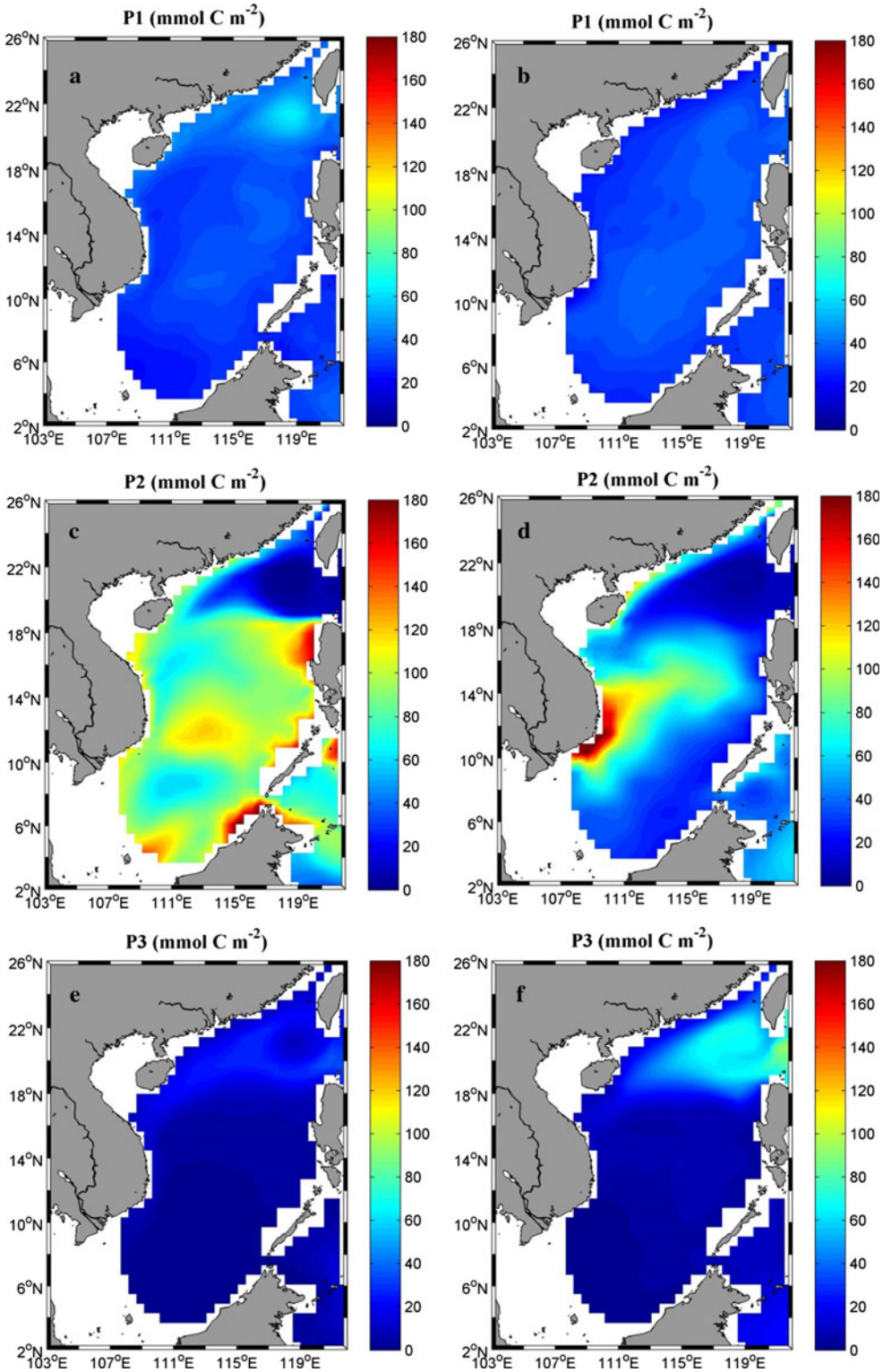

Fig. 6 0–125 m integrated carbon of **a**, P1, **c**, **d** P2, and **e**, **f** P3 in January (*left*) and July (*right*), respectively

SCS, is an important nutrient source to the shelf. The Pearl River plume can occupy a large area of the middle shelf with high concentrations of NO_3 and SiO_4 (Cai et al. 2004; Han et al. 2012). Very high Chl-a concentrations near the Pearl River Estuary in the SeaWiFS data could be the result of high riverine nutrients. Salinity transect showed that fresh water from the Pearl River was able to flush to the shelf break during wet seasons (Cai et al. 2004). Thus, the lateral advection and mixing may bring more nutrients to the northern basin. These high riverine nutrients can

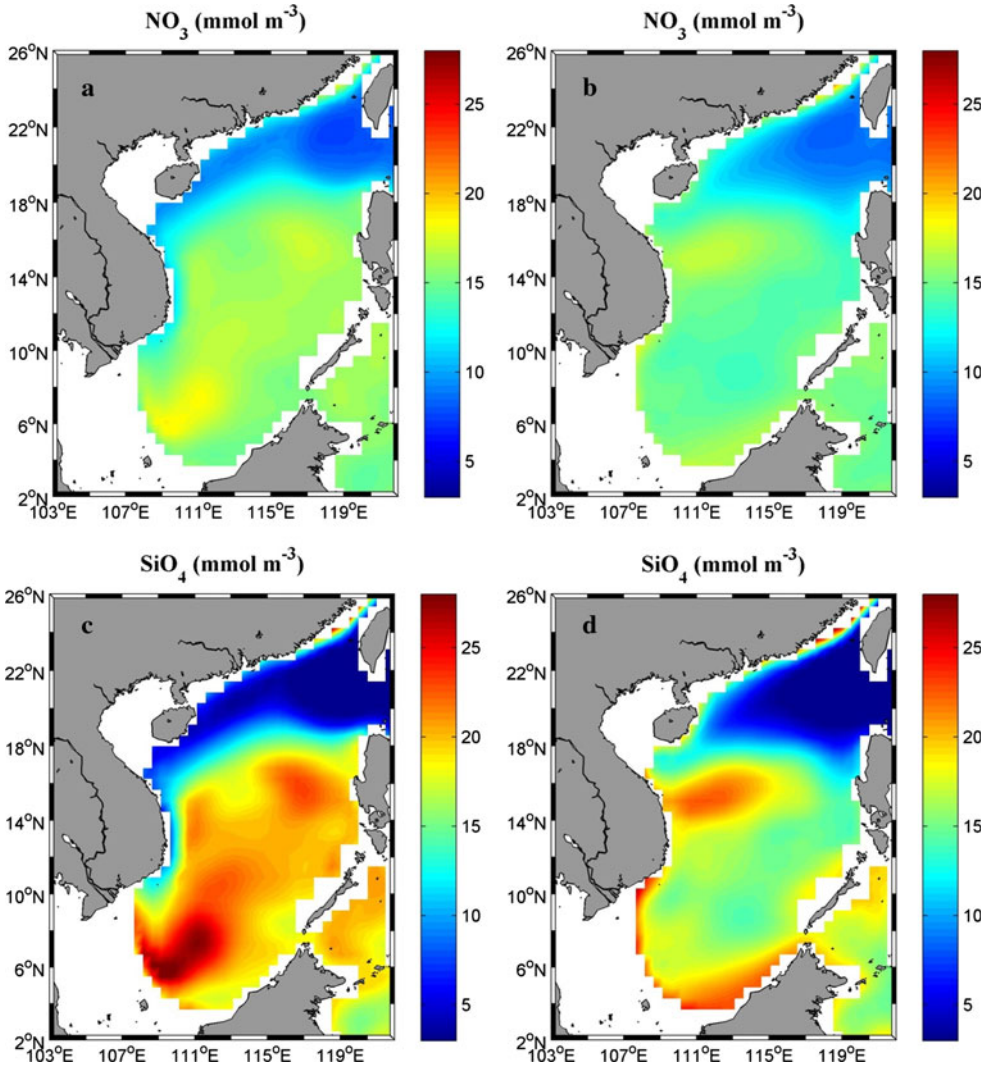

Fig. 7 SiO_4 (**a**, **b**) and NO_3 (**c**, **d**) concentration at 125 m in January (*left*) and July (*right*), respectively

support the growth of phytoplankton not only in the estuary but also on the shelf and adjacent deep sea.

The third possible reason is the insufficient horizontal resolution of the model. More than 30 eddies in the SCS were identified each year by a similar model, but with a 12.5-km resolution in the horizontal (Xiu et al. 2010). The northern SCS is the place where mesoscale eddies occur with high frequencies (Li et al. 2011; Xiu et al. 2010). The upwelling associated with cyclonic eddies is an important mechanism to enhance PP on the route of eddies (Xiu and Chai 2011). Our current model configuration with a horizontal resolution of 50 km is not adequate to resolve the impact of eddies.

3.2 Spatial distribution of the modeled phytoplankton

Satellites detect the backscattering optical signal from the ocean surface. Therefore, Chl-a concentration derived from SeaWiFS only reflected the condition in a few of the surface layers. The SCM, however, is a widespread feature in the subtropics (Hense and Beckmann 2008; Perez et al. 2006; Radenac and Rodier 1996). It occurs at the depth of ~75 m in the SCS (Ning et al. 2004). Surface backscattering based on remote sensing probably contains large uncertainties in the estimation of biomass and PP. Incorporating a variable Chl-a/N ratio into the latest ROMS–CoSiNE model allowed us to reproduce SCM better compared with the previous study (Liu and Chai 2009). Moreover, the variable C/N rather than fixed Redfield ratio made carbon an independent tracer in this study.

To investigate phytoplankton biomass in the water column, we integrated carbon content of three phytoplankton functional groups from 0 to 125 m, close to the bottom of the euphotic zone in the SCS (Shang et al. 2011). The annual mean phytoplankton compositions in different regions are shown in Table 1 and Fig. 4. The distribution of small phytoplankton was very uniform. Its annual mean carbon concentration, integrated from 0 to 125 m, of the

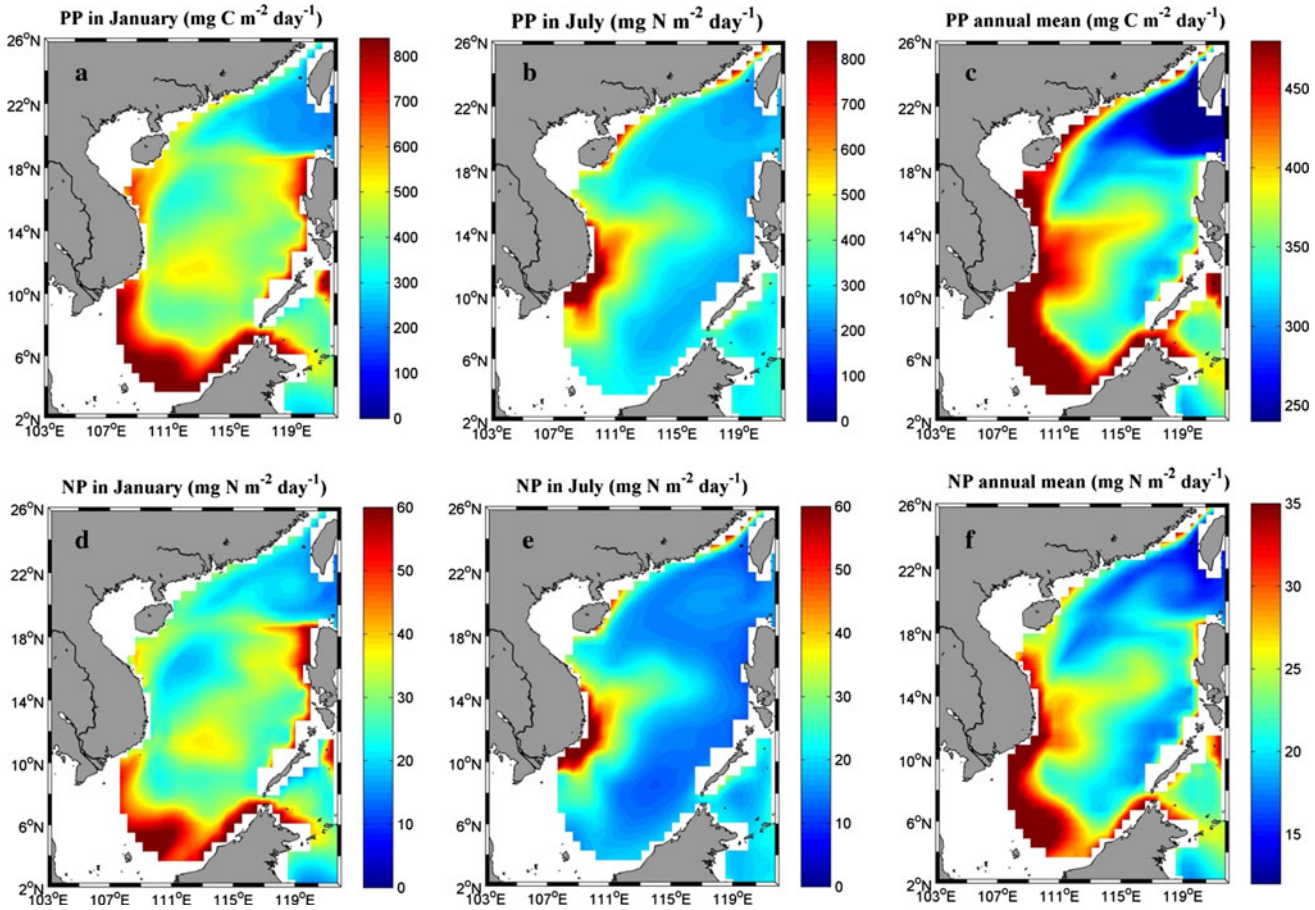

Fig. 8 Modeled primary productivity (PP) (*top panel*) and new production (NP) (*bottom panel*) in January (**a**, **d**), July (**b**, **e**), and annual mean (**c**, **f**)

entire basin was estimated to be ~35 mmol m^{-2} with slightly high values in the northeastern (40.4 mmol m^{-2}) and central basin (36.7 mmol m^{-2}). Diatoms mainly existed in the central and southern basins. High concentration values spread from western Luzon Island to eastern Vietnam. The distribution of annual mean total phytoplankton carbon is similar to that of diatoms, suggesting the dominant group of the biomass comprises diatoms. The concentration of coccolithophores was high in the north and very low in the south. Overall, small phytoplankton, diatoms, and coccolithophores accounted for 33.7, 52.7, and 13.6 % of the biomass, respectively. Picoplankton is thought to be dominant in oligotrophic subtropical waters (Iglesias-Rodríguez et al. 2002; Litchman et al. 2007; Margalef 1978). The field survey by Ning et al. (2004) also reported that picoplankton accounted for 63–77 % in summer and about 52 % in winter. Therefore, the proportion of diatoms may be overestimated in the model.

The composition of three functional groups in different depth showed that the fraction of diatoms and coccolithophores increased with depth while the fraction of small phytoplankton decreased with depth (Fig. 5). The biomass of diatoms and small phytoplankton were nearly equal to each other at the surface but diatoms became more dominant in deeper waters. This decrease of the small phytoplankton fraction with depth was mostly due to its non-sinking treatment in the model. Small phytoplankton did not sink to the subsurface unlike diatoms and coccolithophores. A high phytoplankton carbon concentration in the central basin (Fig. 4d) was likely because of the upwelling-driven nutrient supply allowed the diatoms be more proliferative in the subsurface layer.

The spatial distribution of three functional groups in winter and summer are presented in Fig. 6. Small phytoplankton did not vary greatly between winter and summer. Diatoms, however, showed a significant seasonal variability. In winter, high values appeared in the offshore area of western Luzon Island, the central basin and the northern Sunda Shelf. In summer, high diatom values elongated from the southwestern to the northeastern SCS. Ning et al. (2004) reported that diatom cell abundance was much higher in winter than summer at the basin scale, but was found to be dominant to the east of Vietnam and the deep basin area in summer. The spatial and temporal

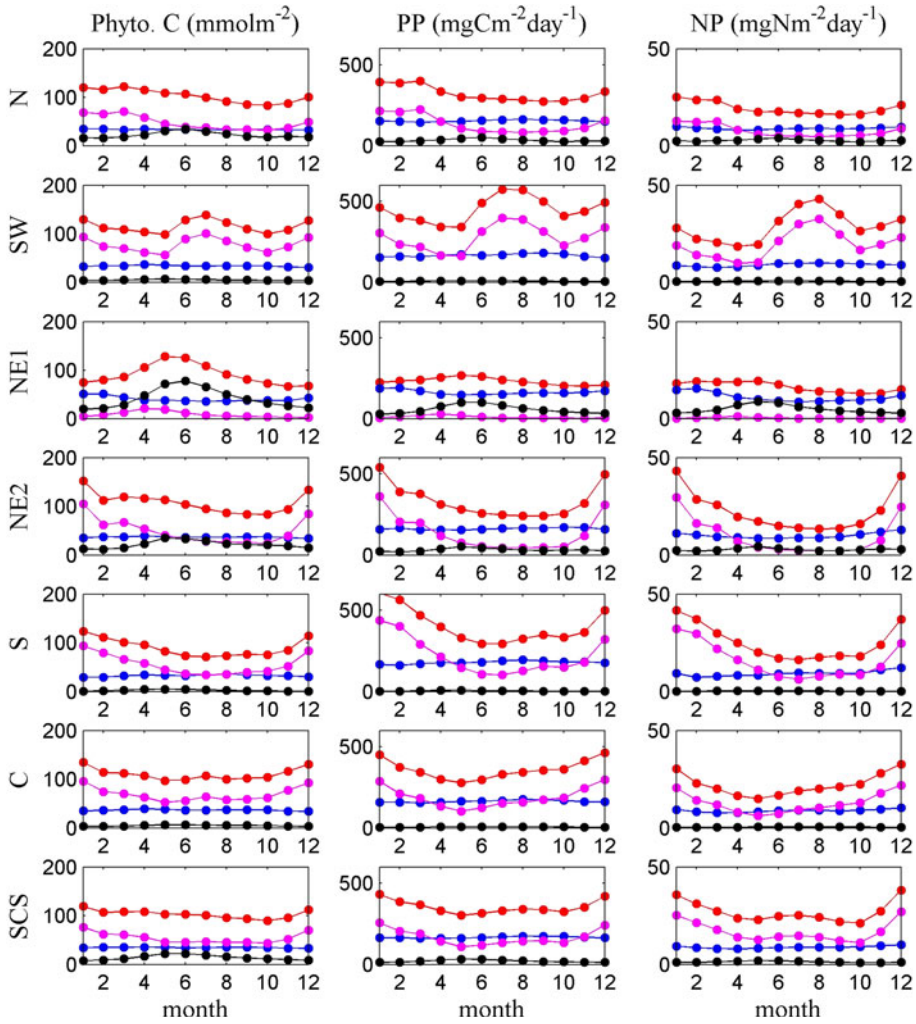

Fig. 9 Climatological annual cycle of phytoplankton carbon (*left*), PP (*middle*), and NP (*right*) averaged in 6 subdomains and the SCS basin. *Black* P3, *blue* P1, *magenta* P3, and *red* P1 + P2 + P3 (color figure online)

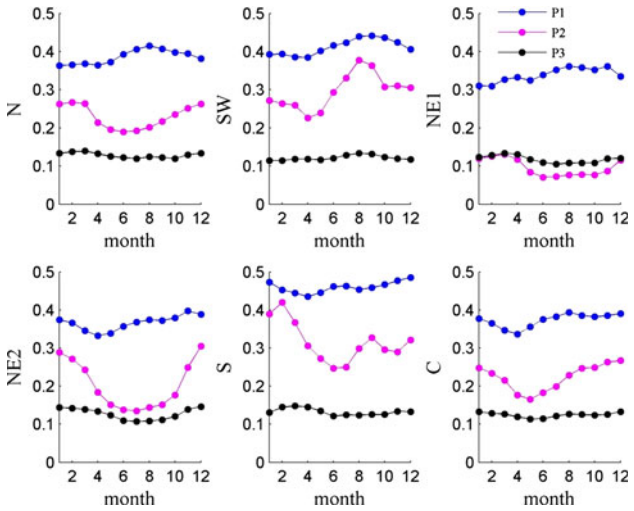

Fig. 10 Climatological annual cycles of phytoplankton specific growth rates in 6 subdomains which are shown in Fig. 4. The unit of the rate is day^{-1}

distributions of diatoms from the model are consistent with this survey. The seasonal variation of coccolithophores showed clearly in the north. Their concentration increased in summer and decreased in winter.

The change of composition in different seasons mainly reflects the variation of nutrient supply. Nutrient concentrations at 125 m represent potential sources for the growth of phytoplankton since these nutrients can reach shallower depth by upwelling and mixing. The low nutrient concentration in the northern SCS in both winter and summer (Fig. 7) probably accounted for the low biomass there. It is worth noting that the variation of coccolithophores reflected the modeled nutrients dynamics. Depleted SiO_4 in the north limited the growth of diatoms. Thus, the relatively enhanced NO_3 to SiO_4 ratio provided room for the growth of coccolithophores and small phytoplankton in the north. Seasonal variations of nutrients also showed its dependence on the EAM. In winter, SiO_4 and NO_3 were noticeably higher than in summer. The northeast winter monsoon

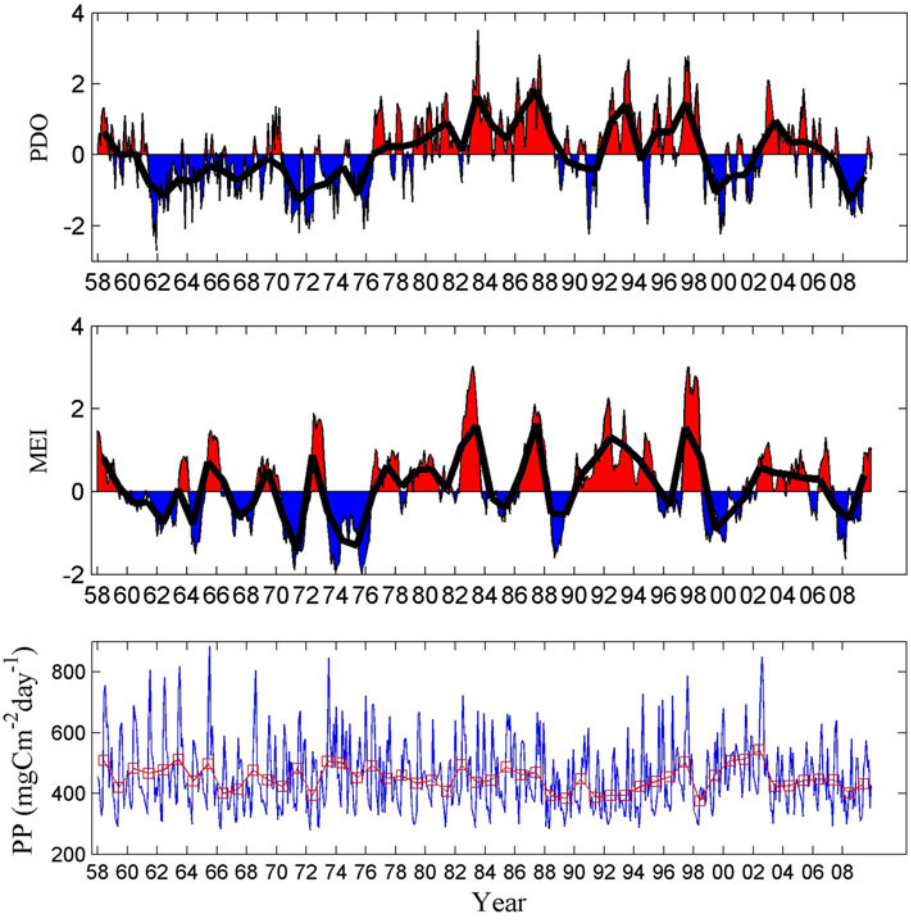

Fig. 11 Comparison of monthly mean of PP in the SW box with multivariable ENSO index (*MEI*) and Pacific decadal oscillation (*PDO*) index from 1958 to 2009. *Black lines* overlaid on the MEI and PDO index and the *red line* on PP denote the corresponding annual mean. MEI is from http://www.esrl.noaa.gov/psd/enso/mei/ and PDO data is from http://jisao.washington.edu/data_sets/pdo/ (color figure online)

resulted in high nutrient values elongating from the southwest to the northeast. As well, more nutrients were found off western Luzon Island, while in summer, high nutrients mainly occurred off eastern Vietnam. Diatoms were more proliferative than other phytoplankton in the areas where SiO_4 is replete. Otherwise, the proportion of diatoms would be low as in the north.

Primary productivity and new production (NP) are two other important variables for evaluating the role of phytoplankton in the biological pump. The definition of NP is the PP supported by new sources of nitrogen (NO_3 in the model). Regenerated production, the counterpart of NP, is supported by forms of recycled nitrogen (NH_4 in the model). NP is thought to equal the export production (the fraction of PP that is exported from the euphotic zone) in the long-term average (Dugdale 1967; Eppley and Peterson 1979). Overall, the vertical integrated PP and NP were consistent with each other in different seasons and annual means (Fig. 8). Maranon et al. (2001) reported the decoupling between phytoplankton carbon and PP in the Atlantic Ocean over a large latitudinal range. In the SCS, however, our modeled results did not show a decoupling. Modeled phytoplankton carbon was consistent with PP and NP probably because the SCS is limited in latitudinal range and does not possess a significant alternation of the community structure.

3.3 Climatological annual cycle of the modeled phytoplankton

We divided the basin into 6 subdomains (see Fig. 4a). Individual months were averaged from 1958 to 2009 to illustrate the climatological seasonal variation. Figure 9 shows the 0–125 m integrated biomass, PP, and NP in these subdomains and the entire basin. At the basin scale, total carbon was higher in winter and lower in summer. Diatoms were consistent with total carbon which was higher in winter, while small phytoplankton and coccolithophores were higher in summer. PP and NP showed more prominent seasonal variations than the biomass. High winter PP and a slightly high summer value were punctuated by two low PP values in May and October, respectively. The similarity between total and diatom carbon indicated that diatoms were the main contributor to the variation of the total biomass. Small phytoplankton and coccolithophores changed less relative to diatoms, but they accounted for a larger proportion from May to October. Nevertheless, the specific growth rate (PP/Phyto. C)

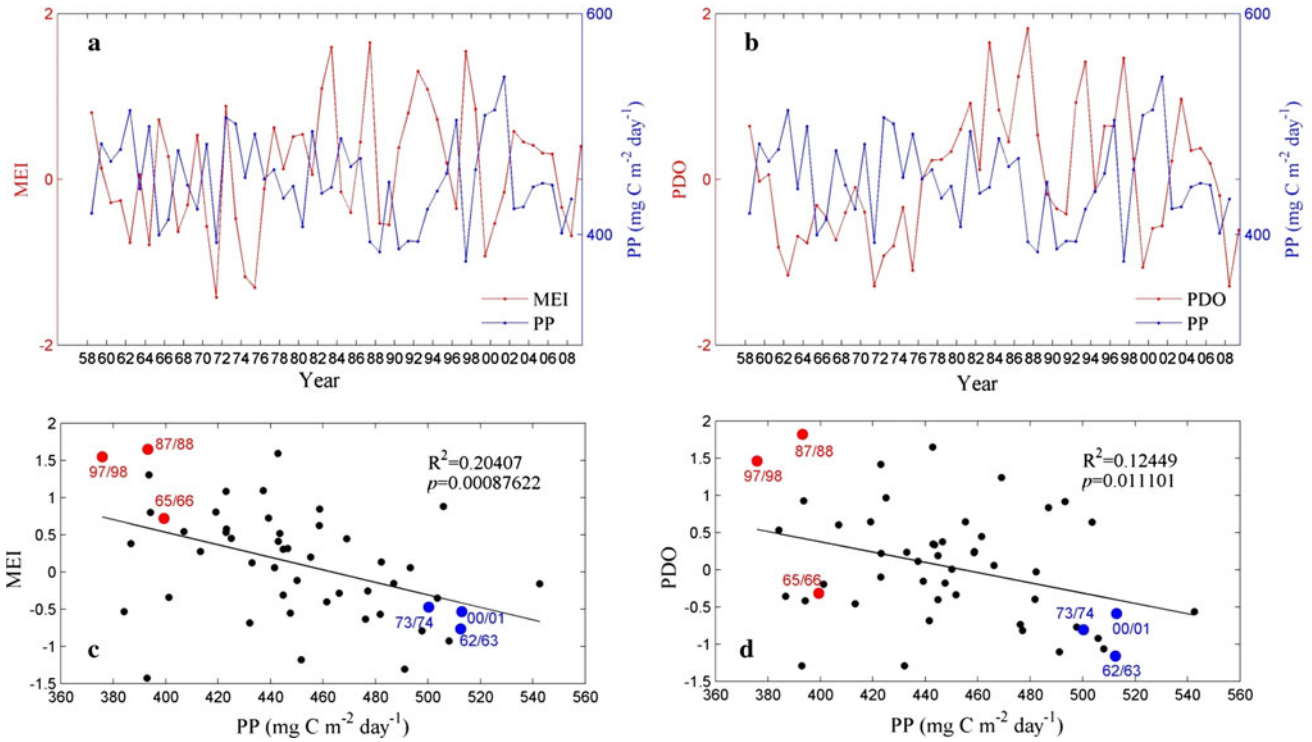

Fig. 12 Comparison of 1-year-lagged annual mean of PP to the MEI and PDO index for the SW box. **a**, **b** The time series of PP versus MEI and PDO index, respectively. **c**, **d** The corresponding scatter plot to (**a**) and (**b**). *Black lines* in (**c**) and (**d**) are the linear regression lines. Three El Niño (*red points*) and La Niña (*blue points*) years are denoted (color figure online)

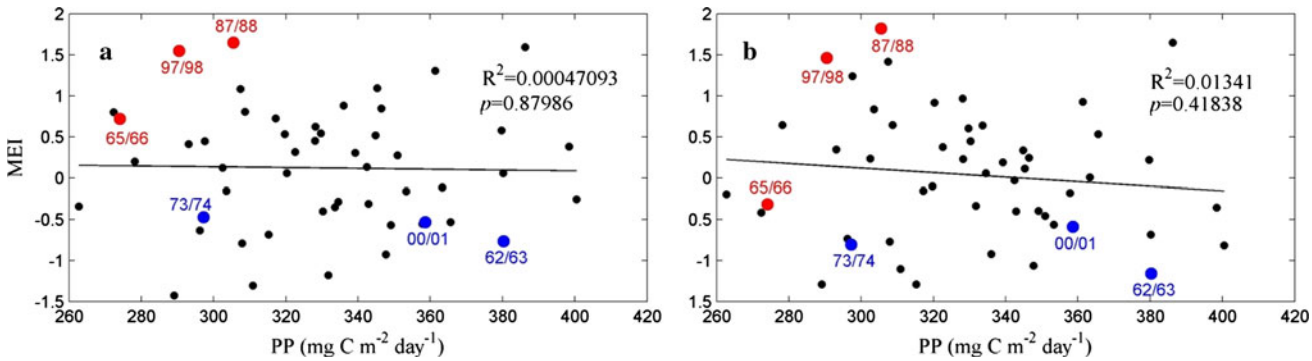

Fig. 13 Scatter plot of 1-year-lagged annual mean PP versus **a** MEI, and **b** PDO index for the NE2 box. *Black lines* are linear regression lines. Three El Niño (*red points*) and La Niña (*blue points*) years are denoted (color figure online)

showed a different pattern compared with either PP or biomass. Small phytoplankton had the highest specific growth rate in each subdomain (Fig. 10). This relatively high specific growth rate and low biomass denoted that the turnover time of small phytoplankton was very rapid and that its standing stock was, however, highly regulated by the grazing pressure of zooplanktons. The specific growth rate of diatoms had larger variations although lower than small phytoplankton.

In the SW box, the modeled PP had two peaks, one in winter and the other in summer; the summer peak was higher than the winter one. In the NE2 and N boxes, PP had only one peak in winter, while in the S and C boxes, winter PP was the highest throughout the year but a weak increase also existed in summer, which was shown more clearly in the specific growth rate. In the N, NE2 and C boxes, PP of small phytoplankton was higher than the other two functional groups from May to November. Due to the depletion of the SiO_4 concentration in the NE1 box, PP of small phytoplankton and coccolithophores were higher than diatoms. This seasonal variation of PP in different boxes clearly showed their link to the alternation of the EAM. The Ekman pumping and enhanced mixing during winter brought more nutrients to the surface especially in the SW

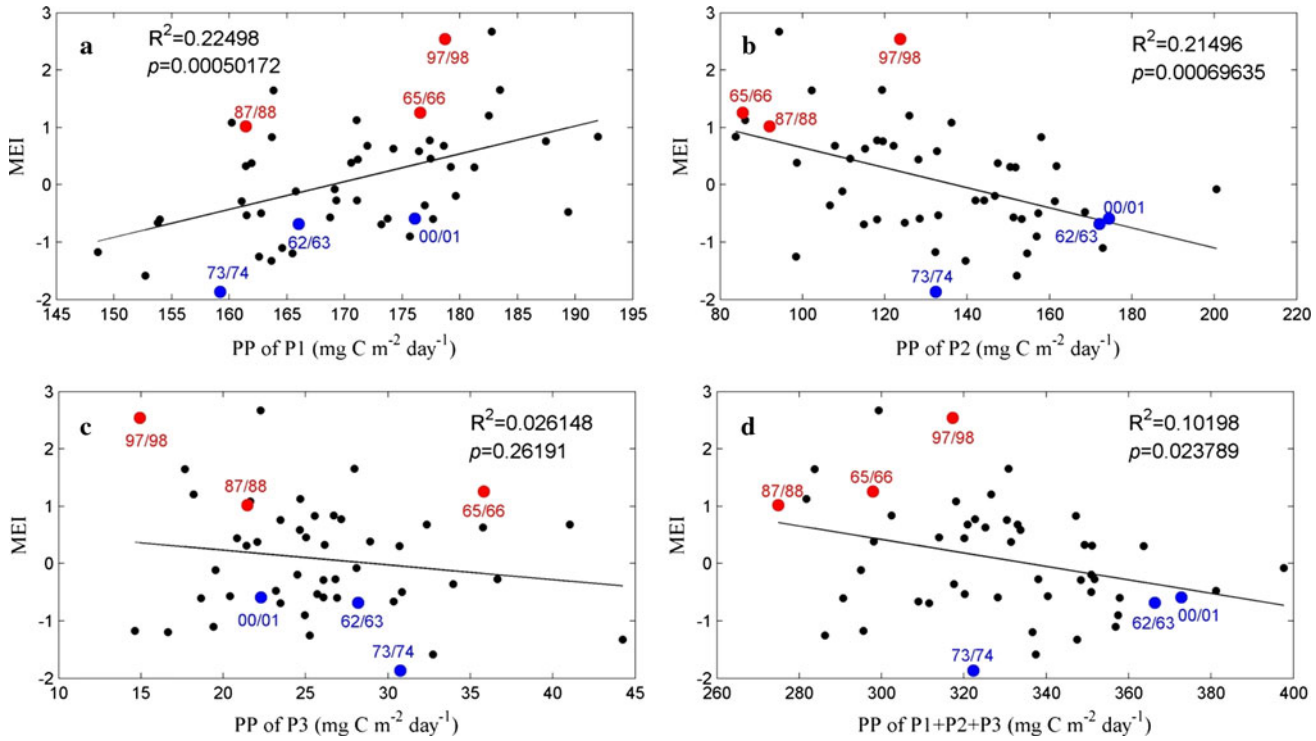

Fig. 14 Scatter plot of MEI versus 6-month-lagged summer (June–August) PP of **a** P1, **b** P2, **c** P3, and **d** P1 + P2 + P3 over the entire SCS. *Black lines* are linear regression lines. Three El Niño (*red points*) and La Niña (*blue points*) years are denoted (color figure online)

Table 2 The model parameters and values

Symbol	Description	Value	Unit
S3	Nitrogen concentration of P3	Model output	mmol N m^{-3} day^{-1}
C3	Carbon concentration of P3	Model output	mmol C m^{-3} day^{-1}
Chl3	Chlorophyll concentration of P3	Model output	mg Chl m^{-3} day^{-1}
Temp	Sea water temperature	Model output	K
K_{NO3}	Half-saturation for NO_3 uptake by P3	1.0	mmol Nm^{-3}
K_{NH4}	Half-saturation for NH_4 uptake by P3	1.0	mmol Nm^{-3}
P_{ref}^{C3}	Maximum coccolithophores carbon-specific nitrogen-uptake	1.0	day^{-1}
Q_{max}	Maximum phytoplankton nitrogen:carbon ratio	0.15	mol N/mol C
Q_{min}	Minimum phytoplankton nitrogen:carbon ratio	0.04	mol N/mol C
Ψ	NH_4 inhibition parameter	5.59	$(\text{mmol N m}^{-3})^{-1}$
ES3	Fraction of new production in dissolved forms	0.1	Dimensionless
α^{Chl3}	Chlorophyll-specific initial slope of P vs. I curve for coccolithophores	0.25	mol C m^2 (g Chl W $day)^{-1}$
$\beta 2$	Mesozooplankton maximum specific grazing rate	0.65	day^{-1}
ζ_{10}	Grazing preference for coccolithophores	0.1	Dimensionless
ζ_5	Grazing preference for diatoms	0.6	Dimensionless
ζ_6	Grazing preference for microzooplankton	0.2	Dimensionless
ζ_7	Grazing preference for detritus	0.1	Dimensionless
θ_{Nmax}^{Chl3}	Maximum value of θ_N^{Chl3}	2.0	g Chl $(\text{mol N})^{-1}$
γ_{10}	Mortality coefficient	0.05	day^{-1}
λ_{S3}	Cost of biosynthesis	2.33	mol C $(\text{mol N})^{-1}$
W3	Coccolithophores sinking velocity	1.0	m day^{-1}

and NE2 boxes. The southwest monsoon in the summer gave rise to enhanced upwelling and mixing not only off Vietnam but also in the southern and central SCS. Sediment traps also showed that the POC and PIC flux had one winter peak in the north and dual peaks (winter and summer) in the south (Chen 2005; Chen et al. 2007a; Wan et al. 2010). The pattern of seasonal variation found in the sediment traps is consistent with our modeled results.

3.4 Interannual variability of PP

Figure 11 shows the time series of monthly mean PP from 1958 to 2009 in comparison with the multivariable El Niño/Southern Oscillation (ENSO) index (MEI) and Pacific decadal oscillation (PDO) index. The modeled PP in the SW box showed a clear semi-annual cycle that was high in both winter and summer but low during transition periods. In addition to the semi-annual cycle, the interannual variability also existed in the PP variation. The 1-year-lagged annual mean PP showed a significant anti-phase relationship with the MEI in the SW box (Fig. 12a, c). The positive phase of ENSO (El Niño) such as 1965/66, 1987/88, and 1997/98 corresponded to low PP values, while the negative phase (La Niña) such as 1962/63, 1973/74, 2000/01 corresponded to higher PP values. Although the annual mean PP also showed a negative relationship with PDO, the correlation was much weaker than that with the ENSO index. In the NE2 box where the higher PP occurred in winter, the modeled PP did not show a good relationship with either ENSO or PDO (Fig. 13).

This spatial difference in the relationship between PP and ENSO is believed to reflect the interaction between the EAM and ENSO. ENSO, which has its mature phase in winter and causes the prominent change of the annual mean MEI in the previous year, plays an important role in modulating the strength of summer monsoon in the successive year. In 1998 for example, the strongest El Niño in recent decades resulted in a significant weakening of the summer monsoon (Lan et al. 2012; Xie et al. 2003, 2009). The summer peak of PP in the southwestern SCS was significantly lower than in normal years. The winter monsoon-driven PP, however, did not show a strong connection with ENSO.

Moreover, the summer PP of three functional groups showed a different relationship to ENSO over the entire basin (Fig. 14). The summer PP of small phytoplankton was positively correlated with ENSO but for diatoms was the reverse. Coccolithophores, however, did not show a significant linear relationship with ENSO. The opposite relationship between small phytoplankton and diatoms in summer revealed that the weak (strong) summer monsoon during El Niño (La Niña) leads to the phytoplankton composition of small phytoplankton (diatoms) being more abundant. In the northern SCS, field observations demonstrated a higher biomass of small phytoplankton in El Niño years (Liu et al. 2007a). Opal and diatom flux was found to be abnormally low during 1987/1988, which corresponded to an El Niño event (Ran et al. 2011). On the other hand, another sediment trap in the central SCS showed a sharp increase of the diatom flux during 1994/1995 (an El Niño event) (Wang et al. 2000). However, this increased diatom flux might be the result of a mesoscale eddy-induced upwelling instead of a basin-wide feature (Ning et al. 2009). Long-term, repeated, and large-scale cruise or sediment trap data are needed to verify the relationship between phytoplankton dynamics and ENSO.

4 Conclusion

We modeled the variation of nutrients, phytoplankton biomass, PP, and composition structure from 1958 to 2009 using the Pacific ROMS–CoSiNE configuration. The modeled chlorophyll and carbon were comparable with the satellite data for the SCS basin. The inconsistency between the modeled results and observations in the northern shelf/slope was due to the overestimated Kuroshio intrusion by the current model, which brought more waters with a low concentration of silicate. Our modeled results indicated that the EAM is responsible for the variations of phytoplankton biomass, PP, and group fractionation, not only at the seasonal but also at the interannual scale. The northeast winter monsoon induces a positive wind stress curl off the west of Luzon Island and on the Sunda Shelf, where upwelling and mixing bring more nutrients to support the growth of phytoplankton. The southwest summer monsoon, on the other hand, drives offshore Ekman transport, hence producing coastal upwelling and high productivity along the coast of southeastern Vietnam.

Annual mean carbon composition of small phytoplankton, diatoms, and coccolithophores was 33.7, 52.7, and 13.6 %, respectively, at the basin scale. The proportion of diatoms was overestimated by the model relative to the small phytoplankton. Diatoms were the main contributor to the seasonal variability of biomass and PP. Small phytoplankton and coccolithophores had less seasonal variability. The peak of diatoms in most subdomains of the SCS occurred in winter except for east of Vietnam, where diatom blooms occurred in both summer and winter. Higher values of small phytoplankton and coccolithophores occurred in summer. Small phytoplankton had the highest specific growth rate but their standing stock is regulated by the high grazing pressure of zooplanktons.

The interannual variability of PP showed that the positive phase of ENSO (El Niño) corresponded to lower PP and the negative phase of ENSO (La Niña) corresponded to higher PP.

Acknowledgments Funding for this research was provided by the NSFC (Grant No. 41206033, 91128208 40976024). This research was also sponsored by Shanghai Shuguang Program (11SG24) and program for New Century Excellent Talents in University (NCET-08-0401). The computation is facilitated by the University of Maine High Performance Computing Center. We are grateful to the two anonymous reviewers for their constructive comments.

Appendix

The model equations of each compartment can be expressed as:

$$\frac{\partial C_i}{\partial t} = \text{Physics}(C_i) + \text{Biology}(C_i), \tag{A1}$$

where C_i ($i = 1, 2, \ldots, 13$) denotes each of the 13 compartments listed in Sect. 2. The first term on the right hand side represents physical processes which include vertical/horizontal advection and eddy diffusion. The second term on the right hand side represents biological processes. Fujii et al. (2007) gave detailed equations for small phytoplankton and diatoms. Here, we only show equations of the nitrogen (A2), carbon (A3) and chlorophyll (A4) concentration that represent dynamics of coccolithophores. The short description and corresponding value of parameters are listed in Table 2.

$$\begin{aligned}&\text{Biology}(\text{S3}(z))\left[\text{mmol N m}^{-3}\text{day}^{-1}\right]\\&= \text{NP3}(z) + \text{RP3}(z) - \text{GS3}(z) - \gamma_{10} \times \text{S3}(z)\\&\quad - \frac{\partial}{\partial z}(\text{W3} \times \text{S3}(z)),\end{aligned} \tag{A2}$$

$$\begin{aligned}&\text{Biology}(\text{C3}(z))\left[\text{mmol C m}^{-3}\text{day}^{-1}\right]\\&= (P^{\text{C3}}(z) - \lambda_{\text{S3}} \times \max\left(\frac{\text{NP3}(z)}{\text{NP3}(z) + \text{RP3}(z)}, 0.5\right)\\&\quad \times (\text{NP3}(z) + \text{RP3}(z))/(1 - \text{ES3})) \times (1 - \text{ES3})\\&\quad - \text{GC3}(z) - \gamma_{10} \times \text{C3}(z) - \frac{\partial}{\partial z}(\text{W3} \times \text{C3}(z)),\end{aligned} \tag{A3}$$

$$\begin{aligned}&\text{Biology}(\text{Chl3}(z))\left[\text{mg Chl m}^{-3}\text{day}^{-1}\right]\\&= (P^{\text{Chl3}}(z) - \text{GChl3}(z) - \gamma_{10} \times \text{Chl3}(z)\\&\quad - \frac{\partial}{\partial z}(\text{W3} \times \text{Chl3}(z)),\end{aligned} \tag{A4}$$

where NP3 and RP3 represent new production and regenerated production, respectively. GS3, GC3, and GChl3 denote the grazing of P3 by Z2 in nitrogen, carbon, and chlorophyll unit, respectively. γ_{10} is the mortality coefficient of P3. The last term in equations A2–A4 represents vertical sinking of P3, and W3 is the sinking velocity. The detailed expressions of biological process are as follows.

New production

$$\begin{aligned}&\text{NP3}(z)\left[\text{mmol N m}^{-3}\text{day}^{-1}\right]\\&= V^{\text{C}}_{\text{NrefS3}} \times e^{-\Psi \text{NH}_4} \times \frac{\text{NO}_3(z)}{K_{\text{NO}_3} + \text{NO}_3(z)}\\&\quad \times T_{\text{func}}(z) \times \frac{1 - f_{\text{nitp3}}(z)}{1.015 - f_{\text{nitp3}}(z)}\\&\quad \times \text{C3}(z) \times (1 - \text{ES3}) \times \left(1 - e^{-\frac{\alpha^{\text{Chl3}}\theta^{\text{C3}}(z)\text{PAR}(z)}{P^{\text{C3}}_{\text{ref}} \times f_{\text{nitp3}}(z) \times T_{\text{func}}(z)}}\right),\end{aligned} \tag{A5}$$

where PAR is photosynthetically active radiation,

$$V^{\text{C}}_{\text{NrefS3}} = P^{\text{C3}}_{\text{ref}} \times Q_{\max}, \tag{A6}$$

$$T_{\text{func}}(z) = \begin{cases} e^{-4000\left(\frac{1}{278.15} - \frac{1}{303.15}\right)}, \text{Temp}(z) < 278.15 \\ e^{-4000\left(\frac{1}{298.15} - \frac{1}{303.15}\right)}, \text{Temp}(z) > 298.15 \\ e^{-4000\left(\frac{1}{\text{Temp}(z)} - \frac{1}{303.15}\right)}, 278.15 \le \text{Temp}(z) \le 298.15 \end{cases}, \tag{A7}$$

$$f_{\text{nitp3}}(z) = \frac{\frac{\text{S3}(z)}{\text{C3}(z)} - Q_{\min}}{Q_{\max} - Q_{\min}}, \tag{A8}$$

$$\theta^{\text{C3}}(z) = \text{Chl3}(z)/\text{C3}(z), \tag{A9}$$

Regenerated production

If $\frac{\text{S3}(z)}{\text{C3}(z)} \le Q_{\min}$,

$$\begin{aligned}&\text{RP3}(z)\left[\text{mmol N m}^{-3}\text{day}^{-1}\right]\\&= V^{\text{C}}_{\text{NrefS3}} \times \frac{\text{NH}_4(z)}{K_{\text{NH}_4} + \text{NH}_4(z)} \times T_{\text{func}}(z)\\&\quad \times \frac{1 - f_{\text{nitp3}}(z)}{1.015 - f_{\text{nitp3}}(z)} \times \text{C3}(z) \times (1 - \text{ES3}),\end{aligned} \tag{A10}$$

If $\frac{\text{S3}(z)}{\text{C3}(z)} > Q_{\min}$,

$$\begin{aligned}&\text{RP3}(z)\left[\text{mmol N m}^{-3}\text{day}^{-1}\right]\\&= V^{\text{C}}_{\text{NrefS3}} \times \frac{\text{NH}_4(z)}{K_{\text{NH}_4} + \text{NH}_4(z)} \times T_{\text{func}}(z) \times \frac{1 - f_{\text{nitp3}}(z)}{1.015 - f_{\text{nitp3}}(z)}\\&\quad \times C3(z) \times (1 - \text{ES3}) \times \left(1 - e^{-\frac{\alpha^{\text{Chl3}}\theta^{\text{C3}}(z)\text{PAR}(z)}{P^{\text{C3}}_{\text{ref}} \times f_{\text{nitp3}}(z) \times T_{\text{func}}(z)}}\right),\end{aligned} \tag{A11}$$

Grazing by Z2

$$\begin{aligned}\text{GS3}(z)\left[\text{mmol N m}^{-3}\text{day}^{-1}\right] &= \beta 2 \times \zeta_{10} \times \text{S3}(z)\\&\quad \times \frac{\text{Z2}(z)}{K_{\text{Z2}} + \zeta_8 + \zeta_9} \times \text{S3}(z),\end{aligned} \tag{A12}$$

$$\mathrm{GC3}(z)\left[\mathrm{mmol\ C\ m^{-3}day^{-1}}\right] = \beta 2 \times \zeta_{10} \times \mathrm{S3}(z) \times \frac{\mathrm{Z2}(z)}{K_{\mathrm{Z2}} + \zeta_8 + \zeta_9} \times \mathrm{C3}(z), \quad \text{(A13)}$$

$$\mathrm{GChl3}(z)\left[\mathrm{mg\ Chl\ m^{-3}day^{-1}}\right] = \beta 2 \times \zeta_{10} \times \mathrm{S3}(z) \times \frac{\mathrm{Z2}(z)}{K_{\mathrm{Z2}} + \zeta_8 + \zeta_9} \times \mathrm{Chl3}(z), \quad \text{(A14)}$$

where

$$\zeta_8 = \zeta_5 \times \mathrm{S2}(z) + \zeta_6 \times \mathrm{Z2}(z) + \zeta_7 \times \mathrm{DN}(z) + \zeta_{10} \times \mathrm{S3}(z), \quad \text{(A15)}$$

$$\zeta_9 = \zeta_5 \times \mathrm{S2}^2(z) + \zeta_6 \times \mathrm{Z2}^2(z) + \zeta_7 \times \mathrm{DN}^2(z) + \zeta_{10} \times \mathrm{S3}^2(z), \quad \text{(A16)}$$

Carbon uptake

$$P^{\mathrm{C3}}(z)\left[\mathrm{mmol\ C\ m^{-3}day^{-1}}\right] = P^{\mathrm{C3}}_{\mathrm{ref}} \times f_{\mathrm{nitp3}}(z) \times T_{\mathrm{func}}(z) \times \left(1 - e^{-\frac{\alpha^{\mathrm{Chl3}}\theta^{\mathrm{C3}}(z)\mathrm{PAR}(z)}{P^{\mathrm{C3}}_{\mathrm{ref}} \times f_{\mathrm{nitp3}}(z) \times T_{\mathrm{func}}(z)}}\right) \times \mathrm{C3}(z), \quad \text{(A17)}$$

Chlorophyll uptake

$$P^{\mathrm{Chl3}}(z)\left[\mathrm{mg\ Chl\ m^{-3}day^{-1}}\right] = \theta^{\mathrm{Chl3}}_{\mathrm{Nmax}} \times \frac{P^{\mathrm{C3}}_{\mathrm{ref}} \times f_{\mathrm{nitp3}}(z) \times T_{\mathrm{func}}(z) \times \left(1 - e^{-\frac{\alpha^{\mathrm{Chl3}}\theta^{\mathrm{C3}}(z)\mathrm{PAR}(z)}{P^{\mathrm{C3}}_{\mathrm{ref}} \times f_{\mathrm{nitp3}}(z) \times T_{\mathrm{func}}(z)}}\right)}{\alpha^{\mathrm{Chl3}}\theta^{\mathrm{C3}}(z)\mathrm{PAR}(z)} \times (\mathrm{NP3}(z) + \mathrm{RP3}(z)). \quad \text{(A18)}$$

References

Behrenfeld MJ, Boss E, Siegel DA, Shea DM (2005) Carbon-based ocean productivity and phytoplankton physiology from space. Glob Biogeochem Cycles 19:GB1006. doi:10.1029/2004GB002299

Cai WJ, Dai M, Wang Y, Zhai W, Huang T, Chen S, Zhang F, Chen Z, Wang Z (2004) The biogeochemistry of inorganic carbon and nutrients in the Pearl River estuary and the adjacent Northern South China Sea. Cont Shelf Res 24(12):1301–1319. doi:10.1016/j.csr.2004.04.005

Cermeño P, Dutkiewicz S, Harris RP, Follows M, Schofield O, Falkowski PG (2008) The role of nutricline depth in regulating the ocean carbon cycle. Proc Natl Acad Sci USA 105(51):20344–20349. doi:10.1073/pnas.0811302106

Chai F, Dugdale RC, Peng TH, Wilkerson FP, Barber RT (2002) One-dimensional ecosystem model of the equatorial Pacific upwelling system. Part I: model development and silicon and nitrogen cycle. Deep Sea Res Pt II 49(12–13):2713–2745. doi:10.1016/s0967-0645(02)00055-3

Chai F, Liu G, Xue H, Shi L, Chao Y, Tseng CM, Chou WC, Liu KK (2009) Seasonal and interannual variability of carbon cycle in South China Sea: A three-dimensional physical-biogeochemical modeling study. J Oceanogr 65(5):703–720. doi:10.1007/s10872-009-0061-5

Chao SY, Shaw PT, Wu SY (1996) Deep water ventilation in the South China Sea. Deep Sea Res Pt I 43(4):445–466. doi:10.1016/0967-0637(96)00025-8

Chen J (2005) Biogeochemistry of settling particles in the South China Sea and its significance on paleo-environment studies. Dissertation, Tongji University, Shanghai

Chen CT, Wang SL, Wang BJ, Pai SC (2001) Nutrient budgets for the South China Sea basin. Mar Chem 75(4):281–300. doi:10.1016/s0304-4203(01)00041-x

Chen R, Wiesner MG, Zheng YL, Cheng XR, Jin HY, Zhao QY, Zheng LF (2007a) Seasonal and annual variations of marine sinking particulate flux during 1993–1996 in the central South China Sea. Acta Oceanolog Sin 26(3):33–43

Chen YLL, Chen HY, Chung CW (2007b) Seasonal variability of coccolithophore abundance and assemblage in the northern South China Sea. Deep Sea Res Pt II 54(14–15):1617–1633. doi:10.1016/j.dsr2.2007.05.005

Dugdale RC (1967) Nutrient limitation in the sea: dynamics, identification, and significance. Limnol Oceanogr 12(4):685–695

Dugdale RC, Barber RT, Chai F, Peng TH, Wilkerson FP (2002) One-dimensional ecosystem model of the equatorial Pacific upwelling system. Part II: sensitivity analysis and comparison with JGOFS EqPac data. Deep Sea Res Pt II 49(13–14):2747–2768. doi:10.1016/s0967-0645(02)00056-5

DuRand MD, Olson RJ, Chisholm SW (2001) Phytoplankton population dynamics at the Bermuda Atlantic Time-series station in the Sargasso Sea. Deep Sea Res Pt II 48(8–9):1983–2003. doi:10.1016/s0967-0645(00)00166-1

Eppley RW, Peterson BJ (1979) Particulate organic matter flux and planktonic new production in the deep ocean. Nature 282(5740):677–680. doi:10.1038/282677a0

Eppley RW, Chavez FP, Barber RT (1992) Standing stocks of particulate carbon and nitrogen in the equatorial Pacific at 150°W. J Geophys Res 97(C1):655–661. doi:10.1029/91JC01386

Fujii M, Chai F (2007) Modeling carbon and silicon cycling in the equatorial Pacific. Deep Sea Res Pt II 54(5–7):496–520. doi:10.1016/j.dsr2.2006.12.005

Fujii M, Boss E, Chai F (2007) The value of adding optics to ecosystem models: a case study. Biogeosciences 4(5):817–835. doi:10.5194/bg-4-817-2007

Garcia HE, Locarnini RA, Boyer TP, Antonov JI, Zweng MM, Baranova OK, Johnson DR (2010) Nutrients (phosphate, nitrate, silicate). In: Levitus S (ed) World Ocean Atlas 2009. NOAA Atlas NESDIS 71. US Government Printing Office, Washington, D.C.

Han A, Dai M, Kao S-J, Gan J, Li Q, Wang L, Zhai W, Wang L (2012) Nutrient dynamics and biological consumption in a large continental shelf system under the influence of both a river plume and coastal upwelling. Limnol Oceanogr 57(2):486–502. doi:10.4319/lo.2012.57.2.0486

Hense I, Beckmann A (2008) Revisiting subsurface chlorophyll and phytoplankton distributions. Deep Sea Res Pt I 55(9):1193–1199. doi:10.1016/j.dsr.2008.04.009

Iglesias-Rodríguez MD, Brown CW, Doney SC, Kleypas J, Kolber D, Kolber Z, Hayes PK, Falkowski PG (2002) Representing key phytoplankton functional groups in ocean carbon cycle models: coccolithophorids. Glob Biogeochem Cycles 16(4):1100. doi:10.1029/2001GB001454

Kalnay E, Kanamitsu M, Kistler R et al (1996) The NCEP/NCAR 40-year reanalysis project. Bull Am Meteorol Soc 77(3):437–471

Kuo NJ, Zheng Q, Ho CR (2000) Satellite observation of upwelling along the western coast of the South China Sea. Remote Sens Environ 74(3):463–470. doi:10.1016/s0034-4257(00)00138-3

Lahajnar N, Wiesner MG, Gaye B (2007) Fluxes of amino acids and hexosamines to the deep South China Sea. Deep Sea Res Pt I 54(12):2120–2144. doi:10.1016/j.dsr.2007.08.009

Lan J, Wang Y, Bao Y (2012) Response of the South China Sea upper layer circulation to monsoon anomalies during 1997/1998 El Nino event. Aquat Ecosyst Health Manag 15(1):6–13. doi:10.1080/14634988.2012.645750

Li JX, Zhang R, Jin BG (2011) Eddy characteristics in the northern South China Sea as inferred from Lagrangian drifter data. Ocean Sci 7(5):661–669. doi:10.5194/os-7-661-2011

Litchman E, Klausmeier CA, Schofield OM, Falkowski PG (2007) The role of functional traits and trade-offs in structuring phytoplankton communities: scaling from cellular to ecosystem level. Ecol Lett 10(12):1170–1181. doi:10.1111/j.1461-0248.2007.01117.x

Liu G, Chai F (2009) Seasonal and interannual variability of primary and export production in the South China Sea: a three-dimensional physical–biogeochemical model study. ICES J Mar Sci 66(2):420–431. doi:10.1093/icesjms/fsn219

Liu KK, Chao SY, Shaw PT, Gong GC, Chen CC, Tang TY (2002) Monsoon-forced chlorophyll distribution and primary production in the South China Sea: observations and a numerical study. Deep Sea Res Pt I 49(8):1387–1412. doi:10.1016/s0967-0637(02)00035-3

Liu QY, Jiang X, Xie SP, Liu WT (2004) A gap in the Indo-Pacific warm pool over the South China Sea in boreal winter: seasonal development and interannual variability. J Geophys Res 109:C07012. doi:10.1029/2003JC002179

Liu H, Chang J, Tseng CM, Wen LS, Liu KK (2007a) Seasonal variability of picoplankton in the Northern South China Sea at the SEATS station. Deep Sea Res Pt II 54(14–15):1602–1616. doi:10.1016/j.dsr2.2007.05.004

Liu KK, Chen YJ, Tseng CM, Lin II, Liu HB, Snidvongs A (2007b) The significance of phytoplankton photo-adaptation and benthic–pelagic coupling to primary production in the South China Sea: observations and numerical investigations. Deep Sea Res Pt II 54(14–15):1546–1574. doi:10.1016/j.dsr2.2007.05.009

Locarnini RA, Mishonov AV, Antonov JI, Boyer TP, Garcia HE (2006),World Ocean Atlas 2005, vol 1: temperature. In: Levitus S (ed) NOAA Atlas NESDIS61. US Government Printing Office, Washington, D.C.

Maranon E, Holligan PM, Barciela R, Gonzalez N, Mourino B, Pazo MJ, Varela M (2001) Patterns of phytoplankton size structure and productivity in contrasting open-ocean environments. Mar Ecol Prog Ser 216:43–56. doi:10.3354/meps216043

Margalef R (1978) Life-forms of phytoplankton as survival alternatives in an unstable environment. Oceanol Acta 1(4):493–509

Metzger EJ, Hurlburt HE (1996) Coupled dynamics of the South China Sea, the Sulu Sea, and the Pacific Ocean. J Geophys Res 101(C5):12331–12352. doi:10.1029/95JC03861

Ning X, Chai F, Xue H, Cai Y, Liu C, Shi J (2004) Physical-biological oceanographic coupling influencing phytoplankton and primary production in the South China Sea. J Geophys Res 109:C10005. doi:10.1029/2004JC002365

Ning X, Lin C, Hao Q, Liu C, Le F, Shi J (2009) Long term changes in the ecosystem in the northern South China Sea during 1976–2004. Biogeosciences 6(10):2227–2243. doi:10.5194/bg-6-2227-2009

Palacz AP, Xue HJ, Armbrecht C, Zhang CY, Chai F (2011) Seasonal and inter-annual changes in the surface chlorophyll of the South China Sea. J Geophys Res 116:C09015. doi:10.1029/2011JC007064

Perez V, Fernandez E, Maranon E, Moran XAG, Zubkovc MV (2006) Vertical distribution of phytoplankton biomass, production and growth in the Atlantic subtropical gyres. Deep Sea Res Pt I 53(10):1616–1634. doi:10.1016/j.dsr.2006.07.008

Qu T, Song YT, Yamagata T (2009) An introduction to the South China Sea throughflow: its dynamics, variability, and application for climate. Dyn Atmos Oceans 47(1–3):3–14. doi:10.1016/j.dynatmoce.2008.05.001

Radenac MH, Rodier M (1996) Nitrate and chlorophyll distributions in relation to thermohaline and current structures in the western tropical Pacific during 1985–1989. Deep Sea Res Pt II 43(4–6):725–752. doi:10.1016/0967-0645(96)00025-2

Ran L, Zheng Y, Chen J, Chen R, Zheng L, Wiesner M (2011) The influence of monsoon on seasonal changes of diatom fluxes in the northern and central South China Sea. Acta Oceanolog Sin 33:139–145 (in Chinese with English abstract)

Shang S, Lee Z, Wei G (2011) Characterization of MODIS-derived euphotic zone depth: results for the China Sea. Remote Sens Environ 115(1):180–186. doi:10.1016/j.rse.2010.08.016

Shaw PT, Chao SY, Liu KK, Pai SC, Liu CT (1996) Winter upwelling off Luzon in the northeastern South China Sea. J Geophys Res 101(C7):16435–16448. doi:10.1029/96jc01064

Su J (2004) Overview of the South China Sea circulation and its influence on the coastal physical oceanography outside the Pearl River Estuary. Cont Shelf Res 24(16):1745–1760. doi:10.1016/j.csr.2004.06.005

Tseng CM, Wong GTF, Lin II, Wu CR, Liu KK (2005) A unique seasonal pattern in phytoplankton biomass in low-latitude waters in the South China Sea. Geophys Res Lett 32:L08608. doi:10.1029/2004GL022111

Wan S, Jian ZM, Cheng XR, Qiao PJ, Wang RJ (2010) Seasonal variations in planktonic foraminiferal flux and the chemical properties of their shells in the southern South China Sea. Sci China Earth Sci 53(8):1176–1187

Wang X, Chao Y (2004) Simulated sea surface salinity variability in the tropical Pacific. Geophys Res Lett 31:L02302. doi:10.1029/2003GL018146

Wang P, Li Q (2009) The South China Sea: paleoceanography and sedimentology. Springer, New York, p 506

Wang R, Lin J, Zheng L, Chen R, Chen J (2000) Siliceous microplankton fluxes and seasonal variations in the central South China Sea during 1993–1995: monsoon climate and El Niño responses. Chin Sci Bull 45(23):2168–2172. doi:10.1007/bf02886323

Wang J, Tang D, Sui Y (2010) Winter phytoplankton bloom induced by subsurface upwelling and mixed layer entrainment southwest of Luzon Strait. J Mar Syst 83(3–4):141–149. doi:10.1016/j.jmarsys.2010.05.006

Wang G, Xie SP, Qu T, Huang RX (2011) Deep South China Sea circulation. Geophys Res Lett 38:L05601. doi:10.1029/2010GL046626

Wei CL, Lin SY, Sheu DD, Chou WC, Yi MC, Santschi PH, Wen LS (2011) Particle-reactive radionuclides (^{234}Th, ^{210}Pb, ^{210}Po) as tracers for the estimation of export production in the South China Sea. Biogeosciences 8(12):3793–3808. doi:10.5194/bg-8-3793-2011

Wong GTF, Ku TL, Mulholland M, Tseng CM, Wang DP (2007a) The South-East Asian Time-series Study (SEATS) and the biogeochemistry of the South China Sea—an overview. Deep Sea Res Pt II 54(14–15):1434–1447. doi:10.1016/j.dsr2.2007.05.012

Wong GTF, Tseng CM, Wen LS, Chung SW (2007b) Nutrient dynamics and N-anomaly at the SEATS station. Deep Sea Res Pt II 54(14–15):1528–1545. doi:10.1016/j.dsr2.2007.05.011

Xie SP, Xie Q, Wang D, Liu WT (2003) Summer upwelling in the South China Sea and its role in regional climate variations. J Geophys Res 108(C8):3261. doi:10.1029/2003JC001867

Xie SP, Hu KM, Hafner J, Tokinaga H, Du Y, Huang G, Sampe T (2009) Indian Ocean capacitor effect on Indo-Western Pacific climate during the summer following El Niño. J Climate 22(3):730–747. doi:10.1175/2008JCLI2544.1

Xiu P, Chai F (2011) Modeled biogeochemical responses to mesoscale eddies in the South China Sea. J Geophys Res 116:C10006. doi:10.1029/2010JC006800

Xiu P, Chai F (2012) Spatial and temporal variability in phytoplankton carbon, chlorophyll, and nitrogen in the North Pacific. J Geophys Res 117:C11023. doi:10.1029/2012JC008067

Xiu P, Chai F, Shi L, Xue H, Chao Y (2010) A census of eddy activities in the South China Sea during 1993–2007. J Geophys Res 115:C03012. doi:10.1029/2009JC005657

Xue H, Chai F, Pettigrew N, Xu D, Shi M, Xu J (2004) Kuroshio intrusion and the circulation in the South China Sea. J Geophys Res 109:C02017. doi:10.1029/2002JC001724

Zhao H, Tang DL (2007) Effect of 1998 El Niño on the distribution of phytoplankton in the South China Sea. J Geophys Res 112:C02017. doi:10.1029/2006JC003536